ChemPubSoc Europe

DOI: 10.1002/chem.201503357

CHEMISTRY
A European Journal
Full Paper

Nanostructures | *Hot Paper*

Superior Electrochemical Properties of Nanofibers Composed of Hollow $CoFe_2O_4$ Nanospheres Covered with Onion-Like Graphitic Carbon

Young Jun Hong, Jung Sang Cho, and Yun Chan Kang*[a]

Abstract: Nanofibers composed of hollow $CoFe_2O_4$ nanospheres covered with onion-like carbon are prepared by applying nanoscale Kirkendall diffusion to the electrospinning process. Amorphous carbon nanofibers embedded with $CoFe_2$@onion-like carbon nanospheres are prepared by reduction of the electrospun nanofibers. Oxidation of the $CoFe_2$-C nanofibers at 300 °C under a normal atmosphere produces porous nanofibers composed of hollow $CoFe_2O_4$ nanospheres covered with onion-like carbon. $CoFe_2$ nanocrystals are transformed into the hollow $CoFe_2O_4$ nanospheres during oxidation through a well-known nanoscale Kirkendall diffusion process. The discharge capacities of the carbon-free $CoFe_2O_4$ nanofibers composed of hollow nanospheres and the nanofibers composed of hollow $CoFe_2O_4$ nanospheres covered with onion-like carbon are 340 and 930 mA h g^{-1}, respectively, for the 1000th cycle at a current density of 1 A g^{-1}. The nanofibers composed of hollow $CoFe_2O_4$ nanospheres covered with onion-like carbon exhibit an excellent rate performance even in the absence of conductive materials.

Introduction

Multicomponent transition metal oxides have been studied previously, with a focus on overcoming the poor cycling performance of single-element transition metal oxides caused by electrode pulverization induced by the huge volume changes during repeated charge/discharge processes.[1–25] Multicomponent transition metal oxides are converted to fine nanocomposites of single-metal oxides and Li_2O immediately after the first electrochemical conversion reaction.[5–10,26–29] These single-metal oxides offer a buffering effect, accommodating the volume change during the charge/discharge process.[5–11,26–28] In addition, composition tuning of multicomponent transition metal oxides enables control of the energy densities and working voltages of electrodes composed of these materials.[5,6,12–14,26,30–33]

Binary transition metal oxide systems having single and multiple phases have been the subject of previous studies, mainly in search of efficient anode materials for lithium storage applications.[5–32,34–56] Solid solutions of oxides of cobalt and iron components have also been studied in the preparation processes of ceramic materials, because cobalt oxides and iron oxides are both promising anode materials for lithium ion batteries (LIBs).[5–14,24,25,28–33] Nanostructured cobalt ferrite material geometries such as nanotubes,[12] nanosheets,[30] hollow shells,[10,45] and yolk-shells[11,25] have been studied previously, and their cycling performances have been improved by enhancing the structural stability during repeated lithium insertion and desertion processes. Carbon materials such as graphene,[46–50] amorphous carbon,[51] graphitic carbon,[32,52] and carbon nanotubes[53] have also been combined with nanostructured materials to further improve their electrochemical properties by enhancing their electrical conductivities and structural stabilities. Liu and co-workers reported core/shell-structured $CoFe_2O_4$/onion-like C nanocapsules delivering a reversible capacity of 914 mA h g^{-1} at 0.1 C even after 500 cycles.[32] Wu and co-workers reported $CoFe_2O_4$/C composite fibers fabricated through electrospinning, which displayed a stable and reversible capacity of over 490 mA h g^{-1} after 700 cycles at a rate of 2.0 C.[52] Zhang and co-workers reported the synthesis and characterization of mesoporous cobalt ferrite nanospheres crosslinked by carbon nanotubes (CNTs), showing a discharge capacity of 1046 mA h g^{-1} for the 100th cycle at a current density of 0.2 A g^{-1}.[53]

In this study, nanofibers composed of hollow $CoFe_2O_4$ nanospheres covered with onion-like carbon are prepared by applying nanoscale Kirkendall diffusion in the electrospinning process. The effect of the onion-like carbon on the electrochemical properties of the nanofibers composed of hollow $CoFe_2O_4$ nanospheres is also investigated.

Results and Discussion

The formation mechanism of the porous nanofibers composed of hollow $CoFe_2O_4$ nanospheres covered with onion-like carbon is described in Scheme 1. The reduction of composite nanofibers consisting of Co acetate, Fe acetylacetonate, and polyacrylonitrile (PAN), formed by electrospinning under a H_2/

[a] *Y. J. Hong, J. S. Cho, Prof. Y. C. Kang*
Department of Materials Science and Engineering, Korea University
Anam-dong, Seongbuk-gu, Seoul 136-713 (Republic of Korea)
E-mail: yckang@korea.ac.kr

Supporting information for this article is available on the WWW under http://dx.doi.org/10.1002/chem.201503357.

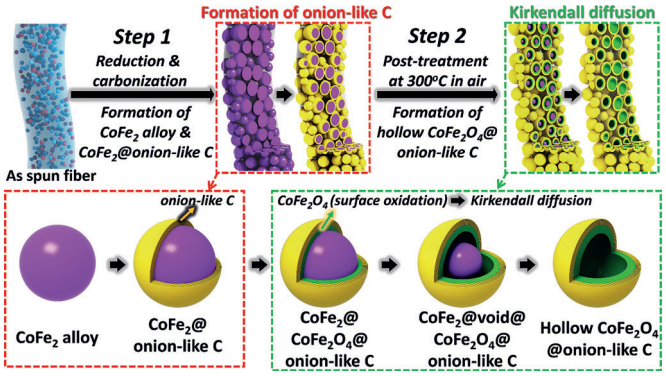

Scheme 1. Schematic diagram of the formation mechanism of the porous nanofibers composed of hollow $CoFe_2O_4$ nanospheres covered with onion-like carbon.

Ar mixed atmosphere, produced carbon nanofibers uniformly embedded with $CoFe_2$ alloy nanocrystals. Decomposition and subsequent reduction of Co and Fe salts distributed uniformly on the electrospun nanofiber formed ultrafine Co and Fe metal nanocrystals. Then, alloying reactions between the Co and Fe metals yielded $CoFe_2$ alloy nanocrystals. The size of the $CoFe_2$ nanocrystals increased with longer reduction time through Ostwald ripening. The carbonization of PAN during reduction formed the amorphous carbon matrix. The amorphous carbon covering the $CoFe_2$ alloy nanocrystals changed into onion-like graphitic carbon during reduction, with the metallic nanocrystals acting as a catalyst.[57–60] Amorphous carbon nanofibers embedded with $CoFe_2$@onion-like C nanospheres with core-shell structures were prepared by reduction of the electrospun nanofibers. Oxidation of the $CoFe_2$-C nanofibers at 300 °C under an air atmosphere produced porous nanofibers composed of hollow $CoFe_2O_4$ nanospheres covered with onion-like carbon. $CoFe_2$ nanocrystals transformed into hollow $CoFe_2O_4$ nanospheres during oxidation through a well-known nanoscale Kirkendall diffusion process.[54–56] Co and Fe cations diffused outward more quickly than oxygen diffused inward, which is consistent with the larger ionic radius of oxygen anions (140 pm) compared with Co and Fe cations (Co^{3+} = 75 pm, Fe^{2+} = 76 pm, Fe^{3+} = 65 pm). Combustion of amorphous carbon during oxidation gave rise to the space between the hollow $CoFe_2O_4$ nanospheres.

On the other hand, the graphitic carbon with onion-like structures remained intact during the oxidation process, and consequently, the electrospun nanofibers were transformed into porous nanofibers composed of hollow $CoFe_2O_4$ nanospheres covered with onion-like carbon in an additional post-treatment step. A detailed formation mechanism of the porous nanofibers composed of hollow $CoFe_2O_4$ nanospheres covered with onion-like carbon was confirmed by investigating the morphologies and crystal structures of the nanofibers obtained in each step. The XRD pattern of the nanofibers, obtained by reduction at 700 °C (shown in Figure S1, Supporting Information), has a sharp peak corresponding to the (110) crystal plane of the CoFe alloy and a broader peak at around 26° attributed to graphitic carbon. $CoFe_2$ solid solution was formed owing to the similar radii and crystalline structures of Co and Fe.[61,62]

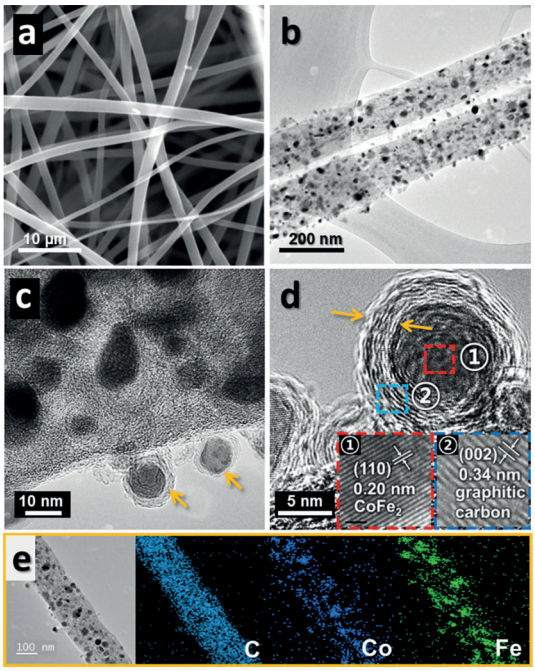

Figure 1. Morphologies and elemental mapping images of the $CoFe_2$-C composite nanofibers obtained after the reduction process: a) SEM image, b,c) TEM images, d) high-resolution TEM image, and e) elemental mapping images.

The morphologies of the $CoFe_2$-C composite nanofibers obtained after the reduction process are shown in Figure 1. The overall morphology of the electrospun nanofibers was maintained even after the reduction process, as shown by the SEM image in Figure 1a. The TEM image in Figure 1b shows that the ultrafine nanocrystals are distributed uniformly all over the semitransparent carbon nanofiber. The ultrafine nanocrystal was uniformly covered with onion-like graphitic carbon, as indicated by the arrows in Figure 1c. The $CoFe_2$ nanocrystal shown in Figure 1d was covered with an onion-like carbon shell (2.7 nm thick). The high-resolution TEM images in the inset image of Figure 1d reveal clear lattice fringes separated by 0.20 and 0.34 nm, which correspond to the (110) crystal plane of the $CoFe_2$ alloy and the (002) crystal plane of graphitic carbon, respectively. The elemental mapping images shown in Figure 1e reveal the distribution of $CoFe_2$ alloy nanocrystals.

The morphologies of the nanofibers, obtained by oxidation of the $CoFe_2$-C composite nanofibers at 300 °C under an air atmosphere for 2 and 10 h, are shown in Figures 2 and 3, respectively, and indicate that the nanofibers display a porous structure. The filled-structure $CoFe_2$-C composite nanofibers were transformed into porous-structured nanofibers after oxidation, owing to the elimination of the amorphous carbon matrix by combustion. However, graphitic carbon was preserved even after 10 h oxidation, as shown by the TEM images in Figure 3c–e. The TEM image shown in Figure 2b displays the yolk-shell-structured nanospheres (nanocrystal@void@shell) that comprise the nanofiber, and the TEM images shown in Figure 3b,c reveal hollow nanospheres that are also present in the nanofiber. The XRD pattern of the nanofibers obtained

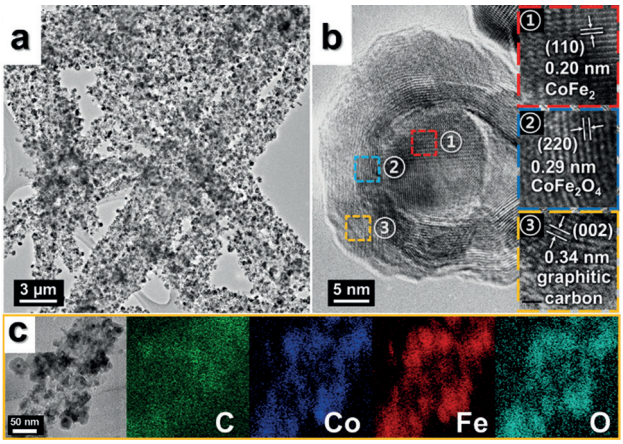

Figure 2. Morphologies and elemental mapping images of the nanofibers obtained after oxidation of the $CoFe_2$-C composite nanofibers at 300 °C under an air atmosphere for 2 h: a) TEM image, b) high-resolution TEM image, and c) elemental mapping images.

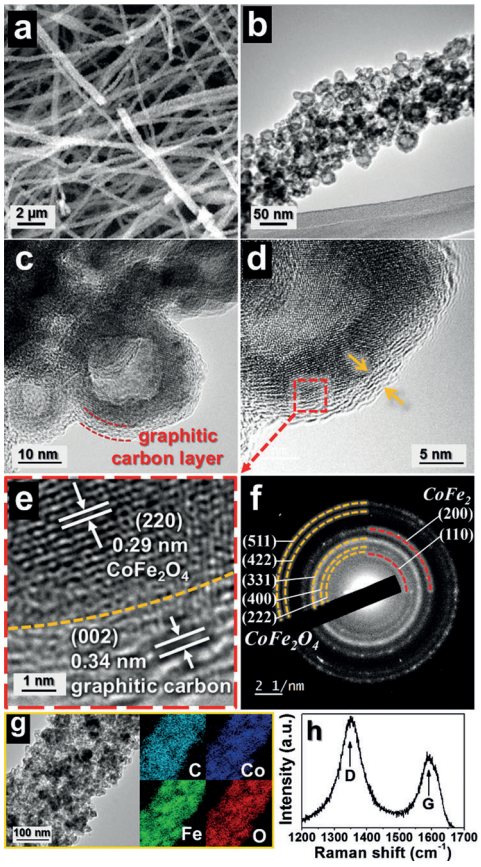

Figure 3. Morphologies, SAED pattern, elemental mapping images, and Raman spectrum of the nanofibers obtained after oxidation of the $CoFe_2$-C composite nanofibers at 300 °C under an air atmosphere for 10 h: a) SEM image, b,c) TEM images, d,e) high-resolution TEM images, f) SAED pattern, g) elemental mapping images, and h) Raman spectrum.

after oxidation for 2 h (Figure S2, Supporting Information) shows crystal peaks attributed to the $CoFe_2O_4$ phase and other, smaller peaks for the $CoFe_2$ alloy phase. The small crystalline peaks of the $CoFe_2$ alloy were also observed in the XRD pattern of the nanofibers obtained after 10 h oxidation, as shown in Figure S2. The conversion of $CoFe_2$ alloy into $CoFe_2O_4$ by oxidation changed the denser precursor structures into hollow spheres through a well-known nanoscale Kirkendall diffusion process (described previously in Scheme 1). Incomplete conversion of $CoFe_2$ alloy nanocrystals into $CoFe_2O_4$ nanospheres during oxidation (2 h) resulted in yolk-shell-structured spheres ($CoFe_2$@void@$CoFe_2O_4$@onion-like C). High-resolution TEM images of the different parts of the nanosphere (Figure 2b) reveal the detailed structure of the yolk-shell nanospheres, and the image of the core part (Figure 2b-1) has clear lattice fringes separated by 0.20 nm, which corresponds to the (110) crystal plane of $CoFe_2$ alloy. TEM images of the interior or exterior shell parts (Figures 2b-2 and b-3) display clear lattice fringes separated by 0.29 and 0.34 nm, which correspond to the (220) crystal plane of $CoFe_2O_4$ and (002) crystal plane of graphitic carbon, respectively. The conversion of $CoFe_2$ alloy nanocrystals into $CoFe_2O_4$ during oxidation (10 h) resulted in hollow-structured nanospheres (void@$CoFe_2O_4$@onion-like C), as shown in Figures 3b,c. The SAED pattern shown in Figure 3f also reveals the formation of $CoFe_2O_4$ nanofibers with small $CoFe_2$ alloy impurities after oxidation at a temperature of 300 °C for 10 h. The elemental TEM images of the interior or exterior shell parts (Figure 3e) portray clear lattice fringes separated by 0.29 and 0.34 nm, which correspond to the (220) crystal plane of $CoFe_2O_4$ and the (002) crystal plane of graphitic carbon, respectively. The mean shell thickness and size of the $CoFe_2O_4$ hollow nanospheres covered with graphitic carbon were measured as 7 and 22 nm, respectively. The mapping images and Raman spectrum (Figure 3g and 3h, respectively) indicate the presence of a carbon material covering the $CoFe_2O_4$ nanospheres. The resonances at 1370 and 1580 cm^{-1} in the Raman spectrum can be assigned to the D- and G-bands of carbon, respectively.[63] The G-band is characteristic of typical graphitic carbon. The graphitic carbon content of the nanofibers composed of hollow nanospheres (void@$CoFe_2O_4$@onion-like C) was estimated as 19.5 wt% in the thermogravimetric (TG) analysis shown in Figure S3 (Supporting Information). The morphologies of the nanofibers obtained after oxidation of the $CoFe_2$-C composite nanofibers at 400 °C under an air atmosphere for 5 h are shown in Figure 4. The nanofibers were composed of hollow nanospheres, as shown by the TEM images in Figure 4b,c. The graphitic carbon covering the hollow nanosphere was not observed in the high-resolution TEM image in Figure 4d. The XRD and SAED patterns shown in Figures S2 and 4f, respectively, reveal the formation of phase-pure $CoFe_2O_4$ nanofibers at an oxidation temperature of 400 °C. The elemental mapping images, TG curve, and Raman spectrum (Figures 4g, S4, and S5, respectively) also demonstrate the formation of carbon-free $CoFe_2O_4$ nanofibers composed of hollow nanospheres. The BET surface area of the $CoFe_2O_4$ nanofibers with hollow nanospheres obtained at oxidation temperatures of 300 °C and 400 °C were 198 and 50 $m^2 g^{-1}$, respectively. The elimination of carbon material and crystal growth of $CoFe_2O_4$ nanospheres at an oxidation temperature of 400 °C decreased the BET surface area. The BJH pore-size distributions of the $CoFe_2O_4$ nanofibers with and

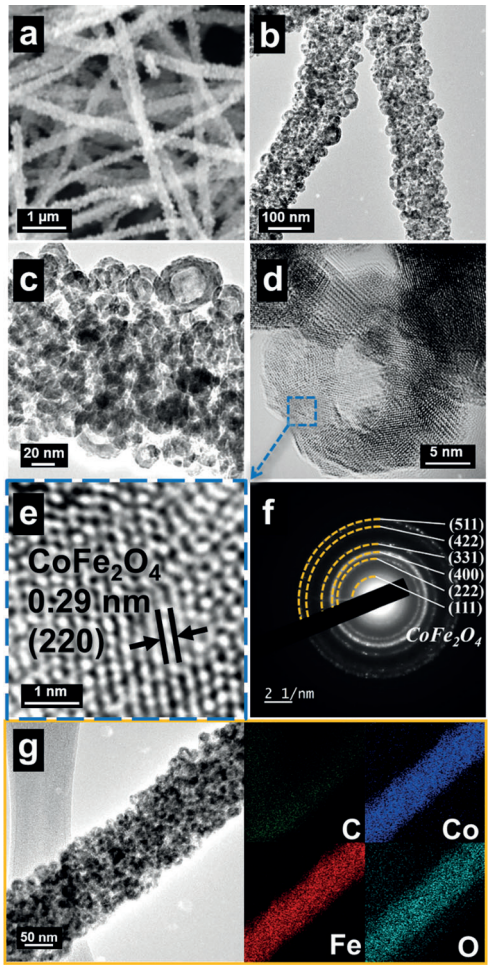

Figure 4. Morphologies, SAED pattern, and elemental mapping images of the nanofibers obtained after oxidation of the $CoFe_2$-C composite nanofibers at 400 °C under an air atmosphere for 5 h: a) SEM image, b,c) TEM images, d,e) high-resolution TEM images, f) SAED pattern, and g) elemental mapping images.

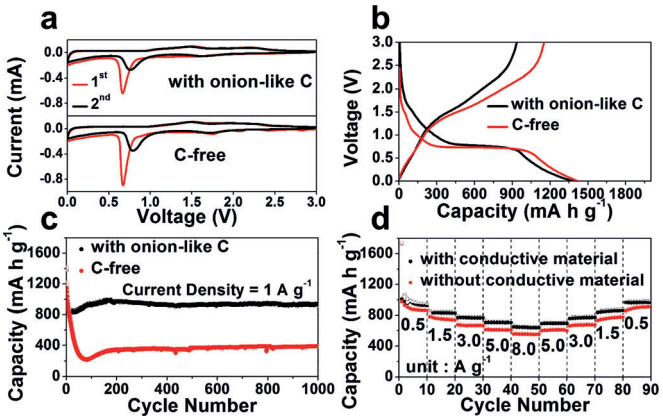

Figure 5. Electrochemical properties of the nanofibers composed of hollow nanospheres (void@$CoFe_2O_4$@onion-like C) and the carbon-free $CoFe_2O_4$ nanofibers composed of hollow nanospheres: a) CV curves, b) initial charge and discharge curves, c) cycling performances, and d) rate performances of the nanofibers composed of hollow nanospheres (void@$CoFe_2O_4$@onion-like C) with and without conductive materials.

without graphitic carbon (shown in Figure S6, Supporting Information) reveal well-developed mesopores with maximum peak intensities of 3.5 and 2–30 nm, respectively.

The electrochemical properties of the $CoFe_2O_4$ nanofibers composed of hollow nanospheres (void@$CoFe_2O_4$@onion-like C) were compared with those of the carbon-free $CoFe_2O_4$ nanofibers composed of hollow nanospheres by means of cyclic voltammetry (CV) and galvanostatic charge/discharge tests in the voltage range 0.001–3 V versus Li/Li^+. The CV curves shown in Figure 5a display a broad single reduction peak at around 0.6 V in the first cathodic scan, corresponding to the reduction of $CoFe_2O_4$ to form metallic nanograins of Co^0 and Fe^0 and amorphous Li_2O, as well as the decomposition of organic electrolyte to form a solid electrolyte interphase (SEI) layer.[10,25,29,52,53] The two broad oxidation peaks observed at 1.6 and 2.2 V in the first charging process of the two samples are attributed to the oxidation of Fe^0 to Fe^{2+} and Fe^{3+}, and Co^0 to Co^{2+} and Co^{3+}, respectively. The reduction peak of the two samples shifted to a higher voltage range of around 0.75 V for the second cycle owing to the formation of ultrafine nanocrystals during the first cycle.[10,25,29,52,53] The initial charge and discharge curves of the two samples at a constant current density of 1 $A g^{-1}$ are shown in Figure 5b. The carbon-free $CoFe_2O_4$ nanofibers composed of hollow nanospheres showed a longer plateau at 0.75 V in the first discharge curve than the nanofibers composed of hollow nanospheres (void@$CoFe_2O_4$@onion-like C). The initial discharge and charge capacities of the carbon-free $CoFe_2O_4$ nanofibers composed of hollow nanospheres were 1420 and 1151 mA h g^{-1}, respectively, and those of the nanofibers composed of hollow nanospheres (void@$CoFe_2O_4$@onion-like C) were 1381 and 936 mA h g^{-1}, respectively. The nanofibers composed of hollow nanospheres (void@$CoFe_2O_4$@onion-like C) had a low initial Coulombic efficiency of 68% owing to the high initial irreversible capacity loss of graphitic carbon. The cycling performances of these two samples at a constant current density of 1 $A g^{-1}$ are shown in Figure 5c. The discharge capacities of the carbon-free $CoFe_2O_4$ nanofibers composed of hollow nanospheres decreased to 285 mA h g^{-1} during the first 90 cycles. The structural degradation caused by repeated lithium insertion/desertion decreased the discharge capacity of the carbon-free $CoFe_2O_4$ nanofibers. However, the discharge capacity of the nanofibers composed of hollow nanospheres (void@$CoFe_2O_4$@onion-like C) increased during the first 160 cycles to 992 mA h g^{-1} thanks to the gradual activation of ultrafine $CoFe_2$ alloys still present in the hollow $CoFe_2O_4$/onion-like C double-shell nanosphere. The nanofibers composed of hollow nanospheres (void@$CoFe_2O_4$@onion-like C) showed excellent cycling performance over the next 840 cycles. The discharge capacities of the carbon-free $CoFe_2O_4$ nanofibers composed of hollow nanospheres and the nanofibers composed of hollow nanospheres (void@$CoFe_2O_4$@onion-like C) for the 1000th cycle were 340 and 930 mA h g^{-1}, respectively. The rate performances of the nanofibers composed of hollow nanospheres (void@$CoFe_2O_4$@onion-like C) are shown in Figure 5d, in which the current density was increased stepwise from 0.5 to 8 $A g^{-1}$, and then decreased stepwise to

0.5 A g^{-1}. The stable reversible discharge capacity of the nanofibers in which conductive material was applied decreased slightly from 960 to 650 mA h g^{-1} as the current density increased from 0.5 to 8.0 A g^{-1}. Furthermore, the discharge capacity recovered well to 980 mA h g^{-1} as the current density was decreased stepwise to 0.5 mA g^{-1}. The nanofibers composed of hollow nanospheres (void@$CoFe_2O_4$@onion-like C) exhibited an excellent rate performance even without conductive material present (Figure 5d). The stable reversible discharge capacity of the nanofibers in which conductive material was not applied decreased slightly from 861 to 550 mA h g^{-1} as the current density increased from 0.5 to 8.0 A g^{-1}. The high electrical conductivity of the nanofibers, attributed to the onion-like graphitic carbon, resulted in superior rate performances for the nanofibers composed of hollow nanospheres (void@$CoFe_2O_4$@onion-like C) with and without conductive materials. The initial Coulombic efficiencies of the nanofibers composed of hollow nanospheres (void@$CoFe_2O_4$@onion-like C) with and without conductive materials were 58.4 and 56.0%, respectively. The carbon black, used as a conductive material, increased slightly the initial Coulombic efficiency of the nanofibers composed of hollow nanospheres (void@$CoFe_2O_4$@onion-like C). Electrochemical impedance spectroscopy (EIS) measurements were performed to explain the superior cycling and rate performances of the nanofibers composed of hollow nanospheres (void@$CoFe_2O_4$@onion-like C). The Nyquist impedance plots obtained before and after cycling are shown in Figure 6. The

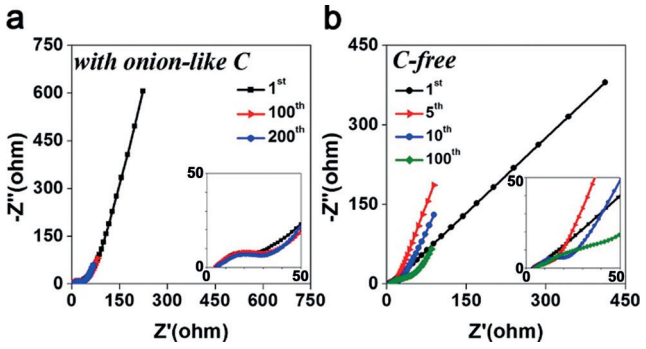

Figure 6. Nyquist impedance plots of a) the nanofibers composed of hollow nanospheres (void@$CoFe_2O_4$@onion-like C) and b) the carbon-free $CoFe_2O_4$ nanofibers composed of hollow nanospheres after cycling.

medium-frequency semicircles in the Nyquist plots of the electrode are assigned to the charge-transfer resistance (R_{ct}).[29] The charge-transfer resistance of the two samples decreased after the first cycle because of the formation of ultrafine nanocrystals. The charge-transfer resistance of the nanofibers composed of hollow nanospheres (void@$CoFe_2O_4$@onion-like C) varied slightly during the first 200 cycles, as shown in Figure 6a. However, the charge-transfer resistances of the carbon-free $CoFe_2O_4$ nanofibers composed of hollow nanospheres increased with the number of cycles, as seen in Figure 6b. The structural degradation of the carbon-free $CoFe_2O_4$ hollow nanospheres during cycling increased the charge-transfer resistance of the nanofibers, and became increasingly evident in subsequent cycles. However, the flexible graphitic carbon layer covering the $CoFe_2O_4$ hollow nanospheres improved the structural stability of the nanofibers composed of hollow nanospheres (void@$CoFe_2O_4$@onion-like C) during repeated lithium insertion/desertion steps. Therefore, the nanofibers composed of hollow nanospheres (void@$CoFe_2O_4$@onion-like C) show excellent long-term cycling performance at a high current density and a good rate performance.[29]

Conclusion

Nanofibers composed of hollow $CoFe_2O_4$ nanospheres with and without graphitic carbon were prepared by applying nanoscale Kirkendall diffusion in the electrospinning process. The oxidation temperature of the $CoFe_2$-C composite nanofibers was a key factor for the formation of an onion-like graphitic carbon layer covering the hollow $CoFe_2O_4$ nanospheres. The flexible onion-like graphitic carbon greatly improved the electrochemical properties of the nanofibers composed of hollow $CoFe_2O_4$ nanospheres by improving the structural stability during repeated lithium insertion/desertion steps. The nanofibers composed of hollow nanospheres (void@$CoFe_2O_4$@onion-like C) exhibited superior electrochemical properties for lithium-ion storage compared with those composed of hollow $CoFe_2O_4$ nanospheres without graphitic carbon.

Experimental Section

Synthesis of nanofibers composed of hollow $CoFe_2O_4$ nanospheres covered with onion-like carbon

Iron(III) acetylacetonate-cobalt(II) acetate tetrahydrate-polyacrylonitrile [$Fe(acac)_3$-$Co(CH_3COO)_2{\cdot}4H_2O$-PAN] composite nanofibers were prepared through an electrospinning process. The precursor solution for the electrospinning process was prepared by dissolving of $Fe(acac)_3$ (3.6 g), $Co(CH_3COO)_2{\cdot}4H_2O$, and PAN ($M_w$: 150000, 4.5 g) in a solution of *N*,*N*-dimethylformamide (DMF, 50 mL) with vigorous stirring overnight. The prepared solution was loaded at a flow rate of 10 mL h^{-1} into a plastic syringe equipped with a 21-gauge stainless steel nozzle. The solution was subsequently ejected and electrospun onto a drum collector covered with aluminum foil. During the electrospinning process, the distance between the tip and the collector was maintained at 20 cm and the rotation of the drum was maintained at 100 rpm. The applied voltage between the collector and the syringe tip was 25 kV. The resultant $Fe(acac)_3$-$Co(CH_3COO)_2{\cdot}4H_2O$-PAN composite nanofibers were stabilized at 150 °C for 5 h in an air atmosphere. For the nanofibers composed of hollow $CoFe_2O_4$ nanospheres, the reduction process was conducted at 700 °C for 3 h in the presence of a gas mixture of 10% H_2/Ar. The subsequent oxidation was conducted at temperatures of 300 and 400 °C in an air atmosphere.

Characterization

The microstructures of the different nanofibers were observed by field-emission scanning electron microscopy (FE-SEM, Hitachi, S-4800) and field-emission transmission electron microscopy (FE-TEM, JEOL, JEM-2100F). In addition, their crystal phases were evaluated by X-ray diffraction (XRD, X'Pert PRO MPD) using CuK_α radiation ($\lambda = 1.5418$ Å) at the Korea Basic Science Institute (Daegu). The

surface areas of the nanofibers were measured using the Brunauer–Emmett–Teller (BET) method with N_2 as the adsorbate gas. Thermogravimetric analysis (TGA) was performed using a Pyris 1 TGA instrument (Perkin Elmer) over the temperature range 25–700 °C at a heating rate of 10 °C min^{-1} under a static air atmosphere. The Raman spectrum of the nanofibers composed of hollow $CoFe_2O_4$ nanospheres covered with onion-like carbon was obtained on a LabRam HR800 UV Raman microscope (Horiba Jobin-Yvon, France).

Electrochemical measurements

The electrochemical properties of the nanofibers were analyzed by constructing a 2032-type coin cell. The anode was prepared by mixing the active material, carbon black, and sodium carboxymethyl cellulose (CMC) at a weight ratio of 7:2:1. Li metal and microporous polypropylene film were used as the counter electrode and the separator, respectively. The negative electrode using the nanofibers was composed of hollow $CoFe_2O_4$ nanospheres covered with onion-like carbon, with dimensions of 1×1 cm and a mass loading of approximately 1.2 mg cm^{-2} of the active material. The electrolyte consisted of 1 M $LiPF_6$ dissolved in a mixture of fluoroethylene carbonate and dimethyl carbonate (FEC/DMC; 1:1 v/v). The discharge/charge characteristics of the samples were investigated by cycling within the 0.001–3 V potential range at various current densities. Cyclic voltammograms (CVs) were measured at a scan rate of 0.07 mV s^{-1}. The electrochemical impedance spectra of the nanofibers were analyzed over the frequency range 0.1–100 kHz at room temperature with a signal amplitude of 1 mV.

Acknowledgements

This work was supported by a National Research Foundation of Korea (NRF) grant funded by the Korea government (MEST) (No. 2012R1A2A2A02046367).

Keywords: energy storage materials · hollow nanospheres · onion-like carbon · nanostructures · synthesis design

[1] M. Ebner, F. Marone, M. Stampanoni, V. Wood, *Science* **2013**, *342*, 716–720.
[2] K. T. Nam, D.-W. Kim, P. J. Yoo, C.-Y. Chiang, N. Meethong, P. T. Hammond, Y.-M. Chiang, A. M. Belcher, *Science* **2006**, *312*, 885–888.
[3] P. Poizot, S. Laruelle, S. Grugeon, L. Dupont, J.-M. Tarascon, *Nature* **2000**, *407*, 496–499.
[4] P. L. Taberna, S. Mitra, P. Poizot, P. Simon, J.-M. Tarascon, *Nat. Mater.* **2006**, *5*, 567–573.
[5] P. G. Bruce, B. Scrosati, J.-M. Tarascon, *Angew. Chem. Int. Ed.* **2008**, *47*, 2930–2946; *Angew. Chem.* **2008**, *120*, 2972–2989.
[6] J. Cabana, L. Monconduit, D. Larcher, M. R. Palacín, *Adv. Mater.* **2010**, *22*, E170–E192.
[7] M. Li, Y.-X. Yin, C. Li, F. Zhang, L.-J. Wan, S. Xu, D. G. Evans, *Chem. Commun.* **2012**, *48*, 410–412.
[8] M. V. Reddy, G. V. S. Rao, B. V. R. Chowdari, *Chem. Rev.* **2013**, *113*, 5364–5457.
[9] C. Z. Yuan, H. B. Wu, Y. Xie, X. W. Lou, *Angew. Chem. Int. Ed.* **2014**, *53*, 1488–1504; *Angew. Chem.* **2014**, *126*, 1512–1530.
[10] Y. Wang, D. W. Su, A. Ung, J. H. Ahn, G. X. Wang, *Nanotechnology* **2012**, *23*, 055402.
[11] Y. N. Ko, S. B. Park, J.-H. Lee, Y. C. Kang, *RSC Adv.* **2014**, *4*, 40188–40192.
[12] X. Zhang, Y. Xie, Y. F. Sun, Q. Zhang, Q. Zhu, D. Hou, J. Guo, *RSC Adv.* **2015**, *5*, 29837–29841.
[13] F. Teh, Y. Sharma, S. S. Pramana, M. Srinivasan, *J. Mater. Chem.* **2011**, *21*, 14999–15008.
[14] A. K. Rai, J. Gim, T. V. Thi, D. Ahn, S. J. Cho, J. Kim, *J. Phys. Chem. C* **2014**, *118*, 11234–11243.
[15] G. Gao, H. B. Wu, X. W. Lou, *Adv. Energy Mater.* **2014**, *4*, 1400422.
[16] L. Hou, L. Lian, L. Zhang, G. Pang, C. Z. Yuan, X. Zhang, *Adv. Funct. Mater.* **2015**, *25*, 238–246.
[17] M. H. Kim, Y. J. Hong, Y. C. Kang, *RSC Adv.* **2013**, *3*, 13110–13114.
[18] C. T. Cherian, J. Sundaramurthy, M. V. Reddy, P. S. Kumar, K. Mani, D. Pliszka, C. H. Sow, S. Ramakrishna, B. V. R. Chowdari, *ACS Appl. Mater. Interfaces* **2013**, *5*, 9957–9963.
[19] G. Huang, F. Zhang, X. Du, J. Wang, D. M. Yin, L. Wang, *Chem. Eur. J.* **2014**, *20*, 11214–11219.
[20] Y. J. Hong, Y. C. Kang, *Carbon* **2015**, *88*, 262–269.
[21] B. J. Li, H. Q. Cao, J. Shao, M. Qu, *Chem. Commun.* **2011**, *47*, 10374–10376.
[22] Z. C. Bai, N. Fan, C. H. Sun, Z. C. Ju, C. L. Guo, J. Yang, Y. T. Qian, *Nanoscale* **2013**, *5*, 2442–2447.
[23] N. Wang, X. J. Ma, Y. Wang, J. Yang, Y. Qian, *J. Mater. Chem. A* **2015**, *3*, 9550–9555.
[24] P. Lavela, J. L. Tirado, *J. Power Sources* **2007**, *172*, 379–387.
[25] S. Li, A. Li, R. Zhang, Y. He, Y. Zhai, L. Xu, *Nano Res.* **2014**, *7*, 1116–1127.
[26] D. Bresser, E. Paillard, R. Kloepsch, S. Krueger, M. Fiedler, R. Schmitz, D. Baither, M. Winter, S. Passerini, *Adv. Energy Mater.* **2013**, *3*, 513–523.
[27] Y. Sharma, N. Sharma, G. V. S. Rao, B. V. R. Chowdari, *J. Power Sources* **2007**, *173*, 495–501.
[28] Z. J. Ding, B. Yao, J. K. Feng, J. Zhang, *J. Solid State Electrochem.* **2014**, *18*, 19–27.
[29] Y. Sharma, N. Sharma, G. V. S. Rao, B. V. R. Chowdari, *Solid State Ionics* **2008**, *179*, 587–597.
[30] X. Yao, J. H. Kong, X. S. Tang, D. Zhou, C. Y. Zhao, R. Zhou, X. H. Lu, *RSC Adv.* **2014**, *4*, 27488–27492.
[31] Y. L. Xiao, X. M. Li, J. T. Zai, K. Wang, Y. Gong, B. Li, Q. Y. Han, X. F. Qian, *Nano-Micro Lett.* **2014**, *6*, 307–315.
[32] X. G. Liu, N. D. Wu, C. Y. Cui, P. P. Zhou, Y. P. Sun, *J. Alloys Comp.* **2015**, *644*, 59–65.
[33] Z. H. Li, T. P. Zhao, X. Y. Zhan, D. S. Gao, Q. Z. Xiao, G. T. Lei, *Electrochim. Acta* **2010**, *55*, 4594–4598.
[34] Y. H. Xua, G. Q. Jian, Y. H. Liu, Y. J. Zhu, M. R. Zachariah, C. S. Wang, *Nano Energy* **2014**, *3*, 26–35.
[35] Y. H. Xua, G. Q. Jian, M. R. Zachariah, C. S. Wang, *J. Mater. Chem. A* **2013**, *1*, 15486–15490.
[36] Y. H. Wang, Y. Wang, J. Tang, Y. Y. Xia, G. F. Zheng, *J. Mater. Chem. A* **2014**, *2*, 20177–20181.
[37] F. Han, W.-C. Li, C. Lei, B. He, K. Oshida, A.-H. Lu, *Small* **2014**, *10*, 2637–2644.
[38] C. Lei, F. Han, Q. Sun, W.-C. Li, A.-H. Lu, *Chem. Eur. J.* **2014**, *20*, 139–145.
[39] F. Han, L. Ma, Q. Sun, C. Lei, A.-H. Lu, *Nano Energy* **2014**, *7*, 1706–1717.
[40] L. Zhan, S. Q. Wang, L.-X. Ding, Z. Li, H. H. Wang, *Electrochim. Acta* **2014**, *135*, 35–41.
[41] H. Jiang, Y. Hu, S. Guo, C. Yan, P. S. Lee, C. Li, *ACS Nano* **2014**, *8*, 6038–6046.
[42] Y.-Q. Chu, Z.-W. Fu, Q.-Z. Qin, *Electrochim. Acta* **2004**, *49*, 4915–4921.
[43] N. Wang, H. Y. Xu, L. Chen, X. Gu, J. Yang, Y. Qian, *J. Power Sources* **2014**, *247*, 163–169.
[44] P. Lavela, G. F. Ortiz, J. L. Tirado, E. Zhecheva, R. Stoyanova, Sv. Ivanova, *J. Phys. Chem. C* **2007**, *111*, 14238–14246.
[45] H. Guo, T. T. Li, W. W. Chen, L. Liu, X. J. Yang, Y. P. Wang, Y. C. Guo, *Nanoscale* **2014**, *6*, 15168–15174.
[46] P. R. Kumar, P. Kollu, C. Santhosh, K. E. V. Rao, D. K. Kim, A. N. Grace, *New J. Chem.* **2014**, *38*, 3654–3661.
[47] H. Xia, D. D. Zhu, Y. S. Fu, X. Wang, *Electrochim. Acta* **2012**, *83*, 166–174.
[48] S. G. Liu, J. Xie, C. C. Fang, G. S. Cao, T. J. Zhu, X. B. Zhao, *J. Mater. Chem.* **2012**, *22*, 19738–19743.
[49] Y. Zhao, J. Li, Y. H. Ding, L. H. Guan, *J. Mater. Chem.* **2011**, *21*, 19101–19105.
[50] C. T. Zhao, C. Yu, S. H. Liu, J. Yang, X. Fan, J. Qiu, *Part. Part. Syst. Charact.* **2015**, *32*, 91–97.
[51] J. J. Zhou, T. Yang, M. Mao, W. Rena, Q. Li, *J. Mater. Chem. A* **2015**, *3*, 12328–12333.
[52] L. Wu, Q. Xiao, Z. Li, G. Lei, P. Zhang, L. Wang, *Solid State Ionics* **2012**, *215*, 24–28.

[53] Z. Zhang, Y. H. Wang, M. Zhang, Q. Q. Tan, X. Lv, Z. Zhong, F. Su, *J. Mater. Chem. A* **2013**, *1*, 7444 – 7450.
[54] J. S. Cho, Y. J. Hong, Y. C. Kang, *ACS Nano* **2015**, *9*, 4026 – 4035.
[55] J. S. Cho, Y. J. Hong, J.-H. Lee, Y. C. Kang, *Nanoscale* **2015**, *7*, 8361 – 8367.
[56] G. D. Park, J. S. Cho, Y. C. Kang, *Nano Energy* **2015**, *17*, 17 – 26.
[57] S. Wang, X, Huang, Y. He, H. Huang, Y. Wu, L. Hou, X. Liu, T. Yang, J. Zou, B. Huang, *Carbon* **2012**, *50*, 2119 – 2125.
[58] J. Xi, Y. Xia, Y. Y. Xu, J. Xiao, S. Wang, *Chem. Commun.* **2015**, *51*, 10479 – 10482.
[59] J. Liu, B. Yu, Q. K. Zhang, L. Hou, Q. Huang, C. Song, S. Wang, Y. Wu, Y. He, J, Zou, H. Huang, *Nanotechnology* **2015**, *26*, 085601.
[60] B. Zhang, Z. L. Xu, Y. B. He, S. Abouali, M. A. Garakani, E. K. Heidari, F. Y. Kang, J.-K. Kim, *Nano Energy* **2014**, *4*, 88 – 96.
[61] C. Bran, E. M. Palmero, Z.-A. Li, R. P. Real, M. Spasova, M. Farle, M. Vázquez, *J. Phys. D J. Phys. D: Appl. Phys.* **2015**, *48*, 145304.
[62] D. Hunter, W. Osborn, K. Wang, N. Kazantseva, J. Hattrick-Simpers, R. Suchoski, R. Takahashi, M. L. Young, A. Mehta, L. A. Bendersky, S. E. Lofland, M. Wuttig, I. Takeuchi, *Nat. Commun.* **2011**, *2*, 518.
[63] F.-D. Han, B. Yao, Y.-J. Bai, *J. Phys. Chem. C* **2011**, *115*, 8923 – 8927.

Received: August 25, 2015
Published online on ■■ ▮▮, 0000

FULL PAPER

Nanostructures

*Y. J. Hong, J. S. Cho, Y. C. Kang**

■■ – ■■

Superior Electrochemical Properties of Nanofibers Composed of Hollow $CoFe_2O_4$ Nanospheres Covered with Onion-Like Graphitic Carbon

Lithium-ion storage: Nanofibers composed of hollow $CoFe_2O_4$ nanospheres covered with onion-like carbon are prepared by applying nanoscale Kirkendall diffusion in the electrospinning process (see figure). The nanofibers composed of hollow nanospheres (void@$CoFe_2O_4$@onion-like C) exhibit superior electrochemical properties for lithium-ion storage compared with the nanofibers composed of hollow $CoFe_2O_4$ nanospheres without graphitic carbon.